Proceedings of the World Congress on Mechanical, Chemical, and Material Engineering (MCM 2015)
Barcelona, Spain – July 20 - 21, 2015
Paper No. 306

Electro-osmotic Flow Through a Rotating Microchannel

Cheng Qi, Chiu-On Ng
Department of Mechanical Engineering, The University of Hong Kong,
Pokfulam Road, Hong Kong
U3001746@hku.hk; cong@hku.hk

Abstract –An analytical model is presented for electro-osmotic flow through a wide rectangular microchannel rotating about an axis perpendicular to its own. The flow is driven by a steady electric field applied along the channel axis, where the upper and lower walls are charged with uniform but possibly disparate zeta potentials. The aim is to understand the interaction between Coriolis force, pressure gradient, viscous force, and the Lorentz force.

***Keywords*:** electro-osmotic flow; rotating microchannel; secondary flow; EDL-Ekman layer.

1. Introduction

Microfluidic devices have been popular in the fields of biomedicine and micro-electromechanical system (MEMS), in which one advanced method for fluidic transport is to make use of externally applied voltages, known as electro-osmotic (EO) pumping.

In recent applications, a microfluidic system may be mounted on a rotating frame, such as centrifuges often used for flow control or mass separation given the advantages that centrifugation may relieve the problem of Joule heating and dispel bubbles of gas (Duffy et al., 1999). Both EO flow and rotating flow have been extensively studied in the literature either theoretically or experimentally, but EO flow in a rotating environment, however, has received less attention than it deserves.

Chang and Wang (2011) pioneered an analytical study on rotating EO flow. They studied rotation-induced secondary EO flow and its effects under various system rotation speeds. In the present problem, the lateral confinement due to side walls, which is ignored in Chang and Wang (2011), is taken into account, and as a result a transverse pressure gradient is induced so as to give a zero net flux in the transverse direction. We look into effects on the primary and secondary flows as functions of the Debye parameter, the rotating speed, and the zeta potentials on the upper and lower walls. A special boundary layer structure is exhibited when the rotational speed and the Debye parameter are sufficiently large (i.e., when the electric double layer (EDL) and the Ekman layer are both thin layers near each of the two horizontal walls). Inside such a composite layer, called the Ekman-EDL layer, the Coriolis force interacts with the electrokinetics. Under fast rotation, the flow is essentially geostrophic in the core region of the channel, where the viscous and electric forces vanish.

2. Problem Formulation

As shown in Fig. 1, the *x*-axis is defined to be along the longitudinal centerline of the microchannel. The microchannel, whose cross section is rectangular with its width much larger than its height (i.e., a very small height to width aspect-ratio *h/b*), rotates about the *z*-axis at a constant rotational speed Ω. The upper and lower walls of the channel are charged with uniform zeta potentials denoted by ζ_1 and ζ_2, respectively. An electric field **E** is applied purely along the *x*-axis.

Considering a micro length scale, a very low Reynolds number is assumed. Ignoring gravity, for an incompressible, steady and fully developed flow, the governing equations in a rotating frame are

$$\nabla \cdot \mathbf{u} = 0, \tag{1}$$

$$2\rho\boldsymbol{\Omega}\times\mathbf{u}=-\nabla P+\mu\nabla^2\mathbf{u}+\rho_{\mathrm{e}}\mathbf{E}, \tag{2}$$

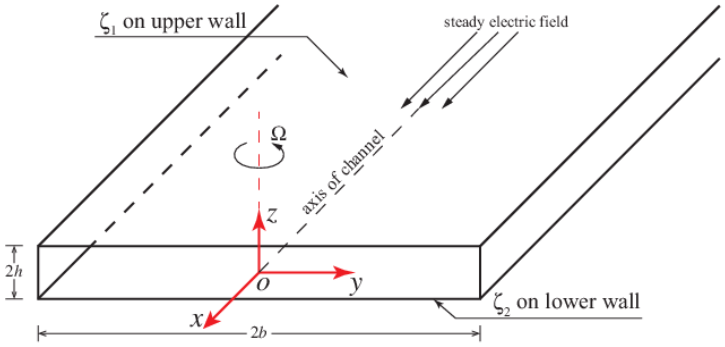

Fig. 1. Schematic diagram of the problem: EO flow through a wide rectangular channel of height $2h$ and width $2b$ rotating about the z-axis with rotational speed Ω with zeta potentials ζ_1 and ζ_2 on its upper and lower walls. A steady electric field is applied along the x-axis.

where ∇ is the gradient operator, $\mathbf{u}=(u,v,0)$ is the velocity vector seen in the rotating frame, $\boldsymbol{\Omega}=(0,0,\Omega)$, $\mathbf{E}=(\mathrm{E},0,0)$, ρ is the fluid density, μ is the dynamic viscosity of the fluid, P is the reduced pressure, and ρ_{e} is the free charge density in the electrolyte.

By electrostatics, the potential distribution $\psi(z)$ in the EDL is related to the free charge density ρ_{e} given by the Poisson equation as

$$\frac{\mathrm{d}^2\psi}{\mathrm{d}z^2}=-\frac{\rho_{\mathrm{e}}}{\varepsilon}, \tag{3}$$

where ε is the dielectric permittivity of the liquid electrolyte. With the further assumptions of a Boltzmann distribution for the ions in the EDL and a symmetrical electrolyte of valence Z, the free charge density is given by

$$\rho_{\mathrm{e}}=-2Zen_\infty\sinh\left(\frac{Ze\psi}{k_BT}\right), \tag{4}$$

where e is the fundamental charge, n_∞ is the bulk concentration, k_B is the Boltzmann constant, and T is the absolute temperature. For a very small potential, combining Eqs. (3) and (4) gives the linearized Poisson-Boltzmann equation

$$\frac{\mathrm{d}^2\psi}{\mathrm{d}z^2}-\kappa^2\psi=0, \tag{5}$$

where $\kappa=(2Z^2e^2n_\infty/\varepsilon k_BT)^{1/2}$ is called the Debye parameter. With the given wall potentials, the potential ψ can be found as

$$\psi(z)=a\frac{\cosh(\kappa z)}{\cosh(\kappa h)}+b\frac{\sinh(\kappa z)}{\sinh(\kappa h)}, \tag{6}$$

where $a=(\zeta_1+\zeta_2)/2$ and $b=(\zeta_1-\zeta_2)/2$. By introducing the following normalized variables and parameters (distinguished by an overhead caret): $\hat{z}=z/h,\ \hat{\kappa}=\kappa h,\ \left(\hat{\psi},\hat{\zeta}_1,\hat{\zeta}_2,\hat{a},\hat{b}\right)=(\psi,\zeta_1,\zeta_2,a,b)/\zeta_0$, where ζ_0 is a reference potential, the potential can be then normalized as

$$\hat{\psi}(\hat{z})=\hat{a}\frac{\cosh(\hat{\kappa}\hat{z})}{\cosh(\hat{\kappa})}+\hat{b}\frac{\sinh(\hat{\kappa}\hat{z})}{\sinh(\hat{\kappa})}, \tag{7}$$

Based on the assumptions made above, the governing equations in a dimensionless form reduce to

$$-\omega\hat{v} = \frac{\mathrm{d}^2\hat{u}}{\mathrm{d}\hat{z}^2} + \hat{\kappa}^2\hat{\psi}, \tag{8}$$

$$\omega\hat{u} = \hat{K}_y + \frac{\mathrm{d}^2\hat{v}}{\mathrm{d}\hat{z}^2}, \tag{9}$$

where $(\hat{u},\hat{v}) = (u,v)/U$ with the scale $U = -\varepsilon\zeta_0 E/\mu$, $\hat{K}_y$ is the pressure gradient along the y-direction, $\omega = 2\rho\Omega h^2/\mu$ is the dimensionless rotation parameter. The solutions $(\hat{u},\hat{v})$ can be readily found as

$$\hat{u}(\hat{z}) = \frac{\hat{K}_y}{\omega} - \hat{a}A\frac{\cosh(\hat{\kappa}\hat{z})}{\cosh(\hat{\kappa})} - \hat{b}A\frac{\sinh(\hat{\kappa}\hat{z})}{\sinh(\hat{\kappa})} + e^{\eta\hat{z}}[C_1\cos(\eta\hat{z}) + C_2\sin(\eta\hat{z})] + e^{-\eta\hat{z}}[C_3\cos(\eta\hat{z}) + C_4\sin(\eta\hat{z})], \tag{10}$$

$$\hat{v}(\hat{z}) = -\hat{a}B\frac{\cosh(\hat{\kappa}\hat{z})}{\cosh(\hat{\kappa})} - \hat{b}B\frac{\sinh(\hat{\kappa}\hat{z})}{\sinh(\hat{\kappa})} + e^{\eta\hat{z}}[C_1\sin(\eta\hat{z}) - C_2\cos(\eta\hat{z})] - e^{-\eta\hat{z}}[C_3\sin(\eta\hat{z}) - C_4\cos(\eta\hat{z})], \tag{11}$$

where $A = \hat{\kappa}^4/(\hat{\kappa}^4 + \omega^2)$ and $B = \omega\hat{\kappa}^2/(\hat{\kappa}^4 + \omega^2)$. The four coefficients $C_{1,2,3,4}$ can be determined by the no-slip boundary condition, while the transverse pressure gradient $\hat{K}_y$ can be determined by the condition of zero transverse net flux.

3. Discussion

It is found that when both $\hat{\kappa}$ and ω are sufficiently large the velocity profile tends to exhibit a boundary-layer structure. This has led us to examine more closely the flow structure in the vicinity of two horizontal walls. We assume here: $\eta \gg 1$ and $\hat{\kappa} \gg 1$ (the ratio of these two large parameter is defined as $\kappa^* = \hat{\kappa}/\eta$, a modified non-dimensional Debye parameter). In this sense, the EDL and Ekman layer are consolidated into a single thin layer, which we may call an Ekman-EDL layer. We define two stretched local coordinates: $\hat{z}_1 = \eta(1 - \hat{z})$, for the layer near the upper wall; $\hat{z}_2 = \eta(1 + \hat{z})$, for the layer near the lower wall.

In terms of these newly defined local coordinates, the expressions of velocity can be rearranged as

$$\hat{u}_1(\hat{z}_1) = \hat{a}(A^* - C^*) - (\hat{a} + \hat{b})A^* e^{-\kappa^*\hat{z}_1} + e^{-\hat{z}_1}[(\hat{a}C^* + \hat{b}A^*)\cos(\hat{z}_1) + (\hat{a} + \hat{b})B^*\sin(\hat{z}_1)], \tag{12}$$

$$\hat{v}_1(\hat{z}_1) = -(\hat{a} + \hat{b})B^* e^{-\kappa^*\hat{z}_1} - e^{-\hat{z}_1}[(\hat{a}C^* + \hat{b}A^*)\sin(\hat{z}_1) - (\hat{a} + \hat{b})B^*\cos(\hat{z}_1)], \tag{13}$$

$$\hat{u}_2(\hat{z}_2) = \hat{a}(A^* - C^*) - (\hat{a} - \hat{b})A^* e^{-\kappa^*\hat{z}_2} + e^{-\hat{z}_2}[(\hat{a}C^* - \hat{b}A^*)\cos(\hat{z}_1) + (\hat{a} - \hat{b})B^*\sin(\hat{z}_2)], \tag{14}$$

$$\hat{v}_2(\hat{z}_2) = -(\hat{a} - \hat{b})B^* e^{-\kappa^*\hat{z}_2} - e^{-\hat{z}_2}[(\hat{a}C^* - \hat{b}A^*)\sin(\hat{z}_2) - (\hat{a} - \hat{b})B^*\cos(\hat{z}_2)], \tag{15}$$

with the definitions of three parameters A^*, B^* and C^*, given as $A^* = \kappa^{*4}/(\kappa^{*4} + 4)$, $B^* = 2\kappa^{*2}/(\kappa^{*4} + 4)$ and $C^* = (\kappa^{*2} - 4\kappa^*)/(\kappa^{*4} + 4)$.

Fig. 2 shows axial and transverse velocity profiles in the vicinity of two horizontal walls for different zeta potential distributions. From Fig. 2 (a) and (b), it is obvious that the axial velocity has an overshoot near the walls and decays to a constant value $\hat{u}_\infty$ in the core region. Theoretically we can obtain this asymptotic limit: $\lim_{\hat{z}_1\to\infty}\hat{u}_1 = \lim_{\hat{z}_2\to\infty}\hat{u}_2 = \hat{a}(A^* - C^*)$, and hence $\hat{u}_\infty = \hat{a}(A^* - C^*)$.

It is obvious that the asymptotic axial velocity $\hat{u}_\infty$ only depends on $\hat{a}$ and κ^*, and is independent on $\hat{b}$. The overshoot of axial velocity is denoted by $\hat{u}_\mathrm{m}$, which may either be positive or negative, and is collectively affected by the zeta potentials on both walls. In Fig. 2 (a), although the zeta potential on the upper wall for all three cases is the same, a larger zeta potential on the lower wall leads to a larger

positive $\hat{u}_{\mathrm{m}}$. In Fig. 2 (b), although the lower wall is not charged for the non-symmetric case (dashed line), there is still an overshoot which may be caused by the zeta potential on the upper wall; the positive $\hat{\zeta}_2$ leads to a larger positive $\hat{u}_{\mathrm{m}}$ and the negative $\hat{\zeta}_2$ leads to a negative $\hat{u}_{\mathrm{m}}$ as the effect of the negative $\hat{\zeta}_2$ overweighs that of the positive $\hat{\zeta}_1$.

As shown in Fig. 2 (c) and (d), the transverse velocity oscillates about the zero value within the Ekman-EDL layer before it decays to zero in the unsheared core region (it can be readily proved that $\lim_{\hat{z}_1\to\infty}\hat{v}_1 = \lim_{\hat{z}_2\to\infty}\hat{v}_2 = 0$), and its integral across the z-direction gives a zero net flow rate. The transverse velocity within the Ekman-EDL layer is affected directly by the rotation-induced Coriolis force and the induced transverse pressure gradient due to electrokinetic effects.

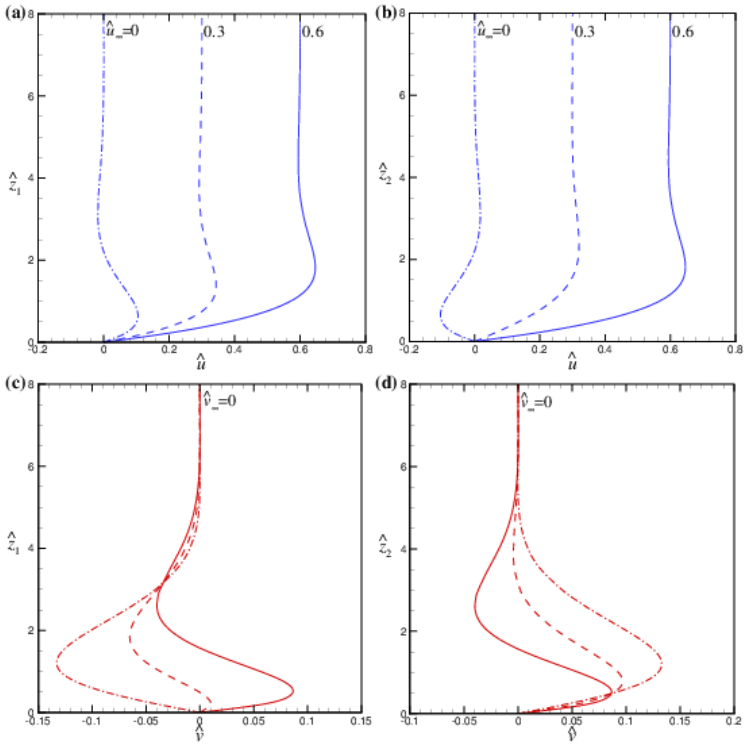

Fig. 2. Velocity profiles within an Ekman-EDL layer formed near the two horizontal walls: (a) axial velocity profile near the upper wall; (b) axial velocity profile near the lower wall; (c) transverse velocity profile near the upper wall; (d) transverse velocity profile near the lower wall, where $\kappa^* = 1$. In each, three cases are shown: (1) $\hat{\zeta}_1 = \hat{\zeta}_2 = 1$ (solid lines); (2) $\hat{\zeta}_1 = 1$ and $\hat{\zeta}_2 = 0$ (dashed lines); (3) $\hat{\zeta}_1 = 1$ and $\hat{\zeta}_2 = -1$ (dash-dot lines).

4. Conclusion

An analytical model for rotating EO flow in a very wide rectangular channel has been developed. We have examined the velocity profiles in the Ekman-EDL layer, which is an electrokinetically modulated Ekman boundary layer that occurs when the Debye and rotation parameters are both large.

Acknowledgements

This work was supported by the Research Grants Council of the Hong Kong Special Administrative Region, China, through Project No. HKU 715510E, and also by the University of Hong Kong through the Small Project Funding Scheme under Project Code 201309176109.

References

Chang, C., & Wang, C. (2011). Rotating Electro-Osmotic Flow Over A Plate Or Between Two Plates. *Phys. Rev. E.*, 84, 056320.

Duffy, D.C., Gillis, H.L., Lin, J., Sheppard, N.F., & Kellogg, G.J. (1999). Microfabricated Centrifugal Microfluidic Systems: Characterization And Multiple Enzymatic Assays. *Anal. Chem.,* 71, 4669-4678.